ISSN: 0067-2904

A comparison of numerical solutions based on two different rates of deformation tensors by using the artificial compressibility method

Bashaer K. Al-Bahrani*, Alaa H. Al-Muslimawi
Department of Mathematics, College of Science, University of Basra, Basra, Iraq

Received: 31/1/2023 Accepted: 29/12/2024 Published: 30/1/2026

Abstract

In this paper, the Newtonian incompressible Navier-Stokes equations in cylindrical polar coordinates can be solved using a Galerkin finite element method proposed based on an artificial compressibility scheme. In this study, two various formulations of the viscous stress tensor are represented, named the rate of deformation tensor T_{rd} and the velocity gradient tensor T_{gv}. A comparison is undertaken between both options T_{rd} and T_{gv}. In this context, attention is paid to the rate of convergence and the influence of variation in Reynolds number (Re) and artificial compressible parameter β_{ac} by using both assumptions, T_{rd} and T_{gv}. The critical values of Reynolds number (Re) and artificial compressible parameter β_{ac} are highlighted in this study as well. Generally, through the analysis of results, we detected that the results with the rate of deformation tensor T_{rd} are better than the results with the velocity gradient tensor T_{gv}.

Keywords: Finite Element Method; Galerkin Method; Artificial Compressibility Method; Newtonian Flow; Navier-Stokes.

مقارنة للحلول العددية تستند إلى معدلين مختلفين من موترات التشوه باستخدام طريقة الانضغاط الاصطناعي

بشائر كاظم البحراني* , علاء حسن المسلماوي
قسم الرياضيات, كلية العلوم, جامعة البصرة, البصرة, العراق

الخلاصة

في هذا البحث ، تم اقتراح طريقة كالركن- العناصر المحدودة لحل معادلات نافييه- ستوكس غير القابلة للضغط النيوتونية في الإحداثيات الأسطوانية بناءً على طريقة الانضغاط الاصطناعي. في هذه الدراسة ، تم تمثيل صيغتين مختلفتين من موتر الإجهاد اللزج ؛ يسمى معدل موتر التشوه (T_{rd}) وموتر تدرج السرعة (T_{gv}). تم إجراء المقارنة بين كلا الخيارين T_{rd} و T_{gv}. في هذا السياق ، يتم إيلاء الاهتمام لمعدل التقارب وتأثير التباين في رقم رينولدز (Re) والمعامل الانضغاطي الاصطناعي (β_{ac}) بأستخدام كلا الافتراضين ؛ T_{rd} و T_{gv}. تم تسليط الضوء على القيم الحرجة لرقم رينولدز (Re) والمعلمة الانضغاطية الاصطناعية (β_{ac}) في هذه الدراسة أيضًا. بشكل عام ، من خلال تحليل النتائج ، اكتشفنا أن النتائج مع معدل موتر التشوه (T_{rd}) أفضل من النتائج مع موتر تدرج السرعة (T_{gv}).

* Email: bashaer.jasim@uobasrah.edu.iq

1. Introduction

The present study is focused on solving the incompressible Navier-Stokes equations for a Newtonian fluid with a special focus on the significance of the stress tensor (T) in determining fluid behavior. The quantities often used in continuum mechanics are the rate of deformation tensor and the spin tensor. These tensors are defined as follows:

$$l = \frac{1}{2}(\nabla u + (\nabla u)^{\tau}), \qquad w = \frac{1}{2}(\nabla u - (\nabla u)^{\tau}),$$

where u is the fluid velocity, see [1], [2], and [3].

Ignoring the torque on an element that is caused by flow (external torque), the viscous 'intrinsic' torque per unit volume of a fluid element is written (as an antisymmetric tensor w), which represents the rate of change in intrinsic angular momentum density during time. When particles have rotational degrees of freedom, they have an intrinsic angular momentum.

This angular momentum can be altered through collisions. The intrinsic angular momentum can change over time, leading to an intrinsic torque that is not zero. As this implies, an antisymmetric component with a corresponding rotational viscosity coefficient will be present in the viscous stress tensor. Conversely, if the fluid particles have negligible angular momentum or their angular momentum is not sufficiently coupled to the external angular momentum, or if the time it takes for the external and internal degrees of freedom to equilibrate is almost zero, then the torque will be zero and the viscous stress tensor will be symmetric (similar to symmetric tensor l). External forces can cause an asymmetric stress tensor component, such as in ferromagnetic fluids that experience torque due to external magnetic fields [4], [5].

In our previous study [6], we studied unsteady incompressible Navier-Stokes equations with deformation rate (T) as velocity gradient tensor. There, the finite element method is employed as a numerical approach based on artificial compressibility to treat the problem under consideration. In addition, the tensor (T) is decomposed into a symmetric and a skewsymmetric part, as

$$d = l + w = \nabla u.$$

To study this subject with a new modification, the same method that was used in our previous investigation is applied with the antisymmetric part of the tensor (T) equal to zero. That is, T only contains the symmetric part (l), and then compares the results for both cases. The novelty of this study is represented by conducting the AC - method in a manner compatible with the Galerkin finite element method under values of the artificial compressible parameter β_{ac}. Moreover, the temporal convergence rate of the system solution is taken under two various formulations of the viscous stress tensor with the effects of β_{ac} and Reynolds number (Re), which was not addressed by researchers previously. Additionally, the determination of the critical Reynolds number levels (Re) is also an exciting issue of this study. As is known, nonlinearity in numerical studies represents a major challenge that needs to be addressed very efficiently. So, the Newton-Raphson method is also applied to treat the nonlinear equations with the backward different scheme within our algorithm.

The mathematical modeling of the motion of Newtonian flows is presented in the next section. These equations are introduced in the cylindrical coordinates. The finite element formulation and the numerical method are characterized in Section 3. In Sections 4 and 5, the problem discretization and related numerical results are shown.

2. Mathematical modelling

The motion equations for a fluid that is incompressible consist of the continuity balance equation, which is defined as:

$$\nabla . u = 0, \tag{1}$$

and momentum balance equation, which is defined based on two different viscous stress tensors, are represented by T_{rd} and T_{gv} (see [3]) :

$$\frac{\partial u}{\partial t} + (u.\nabla)u = \frac{1}{\rho}\nabla.(-pI + T_{rd}), \tag{2}$$

$$\frac{\partial u}{\partial t} + (u.\nabla)u = \frac{1}{\rho}\nabla.\left(-pI + T_{gv}\right). \tag{3}$$

Here, u is the velocity vector, p the hydrodynamic pressure, I is the unit tensor, and T_{rd} and T_{gv} are the viscous stress tensors, such that

$$T_{rd} = \mu_s(\nabla u + (\nabla u)^{\tau}), \quad T_{gv} = \mu_s \nabla u\,,$$

where μ_s is the solvent viscosity.

On the other hand, Equations (2), and (3) can also be defined by the non-dimensional groups, denoted by a^*, are used

$u = Uu^*\ , p = \mu_s \frac{U}{L} p^*,\quad t = \frac{L}{U} t^*,\ L = \frac{U}{L}\ L^*\ ,\ \nabla = \frac{1}{\mathrm{L}}\nabla^*$,

where the scales of U, L, ρ, p and μ_s are velocity, length, density, pressure, and viscosity, respectively, and defined the nondimensional Reynolds number (Re) as $Re = \rho\frac{Ul}{\mu_s}$, see [7-10].

$$\frac{\partial u}{\partial t} + (u.\nabla)u = \frac{1}{Re}\nabla.(-pI + T_{rd}), \tag{4}$$

$$\frac{\partial u}{\partial t} + (u.\nabla)u = \frac{1}{Re}\nabla.\left(-pI + T_{gv}\right). \tag{5}$$

The numerical solution of these equations is a major challenge, due in part to the importance of pressure in the equations. Thus, the Galerkin finite element method based on the artificial compressibility (AC) method is employed to solve the system of governing equations. In this context, the Navier-Stokes equations can be changed to a hyperbolic compressible system, which can be solved by a standard time-dependent approach for more details details, see [11-16]. Here, the continuity equation is rewritten in the form:

$$\frac{1}{\beta_{ac}}\frac{\partial p}{\partial t} + \nabla . u = 0, \tag{6}$$

where, β_{ac} is the artificial compressibility parameter.

2.1 Numerical background

The finite element method has become a popular method for solving incompressible Navier-Stokes equations, see [17]. First, in the cylindrical components, Equations (6) and (4) can be written as

Continuity equation

$$\frac{1}{\beta_{ac}}\frac{\partial p}{\partial t} + \frac{\partial u_r}{\partial r} + \frac{1}{r}u_r + \frac{1}{r}\frac{\partial u_\theta}{\partial \theta} + \frac{\partial u_z}{\partial z} = 0. \tag{7}$$

Momentum equation

r-component

$$\frac{\partial u_r}{\partial t} + u_r\frac{\partial u_r}{\partial r} + \frac{u_\theta}{r}\frac{\partial u_r}{\partial \theta} - \frac{u_\theta^2}{r} + u_z\frac{\partial u_r}{\partial z} = -\frac{1}{Re}\frac{\partial p}{\partial r} + \frac{\beta}{Re}(2\frac{\partial^2 u_r}{\partial r^2} + \frac{2}{r}\frac{\partial u_r}{\partial r} + \frac{1}{r^2}\frac{\partial^2 u_r}{\partial \theta^2} - \frac{1}{r^2}\frac{\partial u_\theta}{\partial \theta} + \frac{1}{r}\frac{\partial^2 u_\theta}{\partial \theta \partial r} + \frac{\partial^2 u_r}{\partial z^2} + \frac{\partial^2 u_z}{\partial z \partial r}), \tag{8}$$

θ-component

$$\frac{\partial u_\theta}{\partial t} + u_r\frac{\partial u_\theta}{\partial r} + \frac{u_\theta}{r}\frac{\partial u_\theta}{\partial \theta} + \frac{u_r u_\theta}{r} + u_z\frac{\partial u_\theta}{\partial z} = -\frac{1}{rRe}\frac{\partial p}{\partial \theta} + \frac{\beta}{Re}(\frac{\partial^2 u_\theta}{\partial r^2} + \frac{1}{r^2}\frac{\partial u_r}{\partial \theta} + \frac{1}{r^2}\frac{\partial^2 u_\theta}{\partial \theta^2} + \frac{\partial^2 u_\theta}{\partial z^2}), \tag{9}$$

z-component

$$\frac{\partial u_z}{\partial t}+u_r\frac{\partial u_z}{\partial r}+\frac{u_\theta}{r}\frac{\partial u_z}{\partial \theta}+u_z\frac{\partial u_z}{\partial z}=-\frac{1}{Re}\frac{\partial p}{\partial z}+\frac{\beta}{Re}(\frac{\partial^2 u_z}{\partial r^2}$$
$$+\frac{1}{r}\frac{\partial u_z}{\partial r}+\frac{1}{r^2}\frac{\partial^2 u_z}{\partial \theta^2}+\frac{\partial^2 u_z}{\partial z^2}). \quad (10)$$

Next, the velocity u and the pressure p are approximated by an interpolation of the nodal point values of the concerned quantity:

$$u(r,\theta,z,t)=\sum_{j=1}^{m_v}\psi_j(r,\theta,z)u_j(t),$$

$$p(r,\theta,z,t)=\sum_{k=1}^{m_p}\phi_k(r,\theta,z)p_k(t),$$

where m_v is the number of velocity nodes and m_p is the number of pressure unknowns ($j=1,2,\ldots,6$, the total number of nodes, which includes mid-side points, and k=1, 2, 3, the number of vertex nodes only).

In matrix-vector notation, Equations (7)-(10) become

$$[M_p][\dot{p}]+[G_1^\tau][u_r]+[g][u_r]+[G_2^\tau][u_\theta]+[G_3^\tau][u_z]=0, \quad (11)$$

$$[M][\dot{u}_r]+[Q(u_r,u_\theta,u_z)][u_r]+[q_\theta][u_\theta]-\frac{1}{Re}[G_1][u_r]+2[C_r][u_r]$$
$$+2[c_r][u_r]+[C_\theta][u_r]+[C_z][u_r]+[f_1][u_\theta]+[f_2][u_\theta]+[H][u_z]=0, \quad (12)$$

$$[M][\dot{u}_\theta]+[Q(u_r,u_\theta,u_z)][u_\theta]+[q_r][u_r]-\frac{1}{Re}[G_2][u_\theta]+[C_r][u_\theta]$$
$$+[C_\theta][u_\theta]+[C_z][u_\theta]-[f_3][u_r]=0, \quad (13)$$

$$[M][\dot{u}_z]+[Q(u_r,u_\theta,u_z)][u_z]-\frac{1}{Re}[G_3][u_z]+[C_r][u_z]+[c_r][u_z]+[C_\theta][u_z]+[C_z][u_z]=0. \quad (14)$$

Such that

1. Mass Matrix,

$$[M]=\int_{\Omega^e}\psi\psi^\tau d\Omega,\ \ [M_p]=\frac{1}{\beta_{ac}}\int_{\Omega^e}\phi\phi^\tau d\Omega. \quad (15)$$

2. Convective Matrix,

$$[Q(u_r,u_\theta,u_z)]=\int_{\Omega^e}(\psi\psi^\tau u_r\frac{\partial\psi^\tau}{\partial r}+\frac{1}{r}\psi\psi^\tau u_\theta\frac{\partial\psi^\tau}{\partial\theta}+\psi\psi^\tau u_z\frac{\partial\psi^\tau}{\partial z})d\Omega, \quad (16)$$

$$[q_\theta]=-\int_{\Omega^e}\frac{1}{r}\psi\psi^\tau u_\theta\psi^\tau d\Omega,\qquad [q_r]=\int_{\Omega^e}\frac{1}{r}\psi\psi^\tau u_\theta\psi^\tau d\Omega.$$

3. Diffusive Matrix,

$$[C_r]=\frac{\beta}{Re}\int_{\Omega^e}\left(\frac{\partial\psi}{\partial r}\frac{\partial\psi^\tau}{\partial r}\right)d\Omega,[c_r]=-\frac{\beta}{Re}\int_{\Omega^e}(\frac{1}{r}\psi\frac{\partial\psi^\tau}{\partial r})d\Omega,[C_\theta]=\frac{\beta}{Re}\int_{\Omega^e}\frac{1}{r^2}\frac{\partial\psi}{\partial\theta}\frac{\partial\psi^\tau}{\partial\theta}d\Omega,$$

$$[C_z]=\frac{\beta}{Re}\int_{\Omega^e}\frac{\partial\psi}{\partial z}\frac{\partial\psi^\tau}{\partial z}d\Omega,\ [f_1]=[f_3]=\frac{\beta}{Re}\int_{\Omega^e}\frac{1}{r^2}\psi\frac{\partial\psi^\tau}{\partial\theta}d\Omega,$$

$$[f_2]=\frac{\beta}{Re}\int_{\Omega^e}\frac{1}{r}\frac{\partial\psi}{\partial r}\frac{\partial\psi^\tau}{\partial\theta}d\Omega. \quad (17)$$

$$[H]=\frac{\beta}{Re}\int_{\Omega^e}\frac{\partial\psi}{\partial z}\frac{\partial\psi^\tau}{\partial r}d\Omega. \quad (18)$$

4. Gradient Matrix,

$$[G_1] = \int_{\Omega^e} \frac{\partial \psi}{\partial r} \phi^\tau d\Omega, [G_2] = \int_{\Omega^e} \frac{1}{r} \frac{\partial \psi}{\partial \theta} \phi^\tau d\Omega, \ [G_3] = \int_{\Omega^e} \frac{\partial \psi}{\partial z} \phi^\tau d\Omega.$$

$$[g] = \int_{\Omega^e} \left(\frac{1}{r} \phi \psi^\tau \right) d\Omega \,. \tag{19}$$

Quadratic and linear triangular shape functions will be utilized for velocities and pressure according to the theory of area coordinates. In this context, the quadratic and linear shape functions for the nature of triangular area coordinates are described:

$$\psi = [A][R], \qquad (Quadratic) \tag{20}$$

$$\phi = [I][E] = [E], \qquad (Linear) \tag{21}$$

where

$$[A] = \begin{bmatrix} 1 & 0 & 0 & -1 & 0 & -1 \\ 0 & 1 & 0 & -1 & -1 & 0 \\ 0 & 0 & 1 & 0 & -1 & -1 \\ 0 & 0 & 0 & 4 & 0 & 0 \\ 0 & 0 & 0 & 0 & 4 & 0 \\ 0 & 0 & 0 & 0 & 0 & 4 \end{bmatrix}, \quad [R] = \begin{bmatrix} L_1^2 \\ L_2^2 \\ L_3^2 \\ L_1 L_2 \\ L_2 L_3 \\ L_3 L_1 \end{bmatrix}, \quad [E] = \begin{bmatrix} L_1 \\ L_2 \\ L_3 \end{bmatrix}. \tag{22}$$

The natural triangular area coordinates L_1, L_2, and L_3 of the cylindrical coordinates are defined as

$$L_i = \frac{1}{2A_{area}} (a_i + b_i r + c_i z), \qquad (i = 1,2,3)$$

where, A_{area} is the area of the element's triangular and a_i, b_i, and c_i are coefficients.

The Equations (11)-(14) can be rewritten in the matrix formulation using these assumptions:

$$\begin{bmatrix} M & 0 & 0 & 0 \\ 0 & M & 0 & 0 \\ 0 & 0 & M & 0 \\ 0 & 0 & 0 & M_p \end{bmatrix} \begin{bmatrix} \dot{u}_r \\ \dot{u}_\theta \\ \dot{u}_z \\ \dot{p} \end{bmatrix} + \begin{bmatrix} K_r & q_\theta & H & \frac{-1}{Re} G_1 \\ q_r & K_\theta & 0 & 0 \\ 0 & 0 & K_z & \frac{-1}{Re} G_3 \\ G_1^\tau + g & 0 & G_3^\tau & 0 \end{bmatrix} \begin{bmatrix} u_r \\ u_\theta \\ u_z \\ p \end{bmatrix} = \begin{bmatrix} 0 \\ 0 \\ 0 \\ 0 \end{bmatrix}, \tag{23}$$

$$[K_r] = [Q_r(u_r)] + [Q_z(u_z)] + 2[C_r] + 2[c_r] + [C_z], \tag{24}$$

$$[K_\theta] = [Q_r(u_r)] + [Q_z(u_z)] + [C_r] + [C_z], \tag{25}$$

$$[K_z] = [Q_r(u_r)] + [Q_z(u_z)] + [C_r] + [c_r] + [C_z]. \tag{26}$$

The mass and artificial compressibility matrix can be expressed by utilizing the theory of area coordinates for triangular elements:

$$[M] = 2\pi r_m A_{area} [A] \underline{[R][R^\tau]} [A^\tau], \tag{27}$$

$$\left[M_p\right] = 2\pi r_m A_{area} \frac{1}{\beta_{ac}} \underline{[E][E^\tau]}, \tag{28}$$

where,

$$r_m = \frac{r_1 + r_2 + r_3}{3}, z_m = \frac{z_1 + z_2 + z_3}{3}. \tag{29}$$

The shape function's derivative form can be defined as:

$$\frac{\partial \psi}{\partial r} = [A][B][E],$$

$$\frac{\partial \psi}{\partial z} = [A][C][E],$$

where,

$$[B] = \begin{bmatrix} 2b_1 & 0 & 0 \\ 0 & 2b_2 & 0 \\ 0 & 0 & 2b_3 \\ b_2 & b_1 & 0 \\ 0 & b_3 & b_2 \\ b_3 & 0 & b_1 \end{bmatrix}, [C] = \begin{bmatrix} 2c_1 & 0 & 0 \\ 0 & 2c_2 & 0 \\ 0 & 0 & 2c_3 \\ c_2 & c_1 & 0 \\ 0 & c_3 & c_2 \\ c_3 & 0 & c_1 \end{bmatrix}.$$

On the other hand, the final diffusion matrix formula can be written as follows:

$$[C_r] = 2\pi r_m A_{area} \frac{\beta}{Re} [A][B]\underline{[E][E^\tau]}[B^\tau][A^\tau], [c_r] = -2\pi A_{area} \frac{\beta}{Re} [A]\underline{[R][E^\tau]}[B^\tau][A^\tau], \quad (30)$$

$$[C_z] = 2\pi r_m A_{area} \frac{\beta}{Re} [A][C]\underline{[E][E^\tau]}[C^\tau][A^\tau], \quad (31)$$

$$[H] = 2\pi r_m A_{area} \frac{\beta}{Re} [A][C]\underline{[E][E^\tau]}[B^\tau][A^\tau], \quad (32)$$

Moreover, the gradient matrix is defined as

$$[G_1] = 2\pi r_m A_{area}[A][B]\underline{[E][E^\tau]}, \quad (33)$$

$$[G_3] = 2\pi r_m A_{area}[A][C]\underline{[E][E^\tau]}, \quad (34)$$

$$[g] = 2\pi A_{area}\underline{[E][R^\tau]}[A^\tau]. \quad (35)$$

The convective matrix is given by

$$[Q_r(u_r)] = 2\pi r_m A_{area}[A]\underline{[R][R^\tau]}[A^\tau][u_r]\underline{[E^\tau]}[B^\tau][A^\tau], \quad (36)$$

$$[Q_z(u_z)] = 2\pi r_m A_{area}[A]\underline{[R][R^\tau]}[A^\tau][u_z]\underline{[E^\tau]}[B^\tau][A^\tau], \quad (37)$$

$$[q_\theta] = -2\pi A_{area}[A]\underline{[R][R^\tau]}[A^\tau][u_\theta]\underline{[R^\tau]}[A^\tau], \quad (38)$$

$$[q_r] = 2\pi A_{area}[A]\underline{[R][R^\tau]}[A^\tau][u_\theta]\underline{[R^\tau]}[A^\tau]. \quad (39)$$

3. Simple test problem

In this study, the model is a very simple channel with a circular cross-section. The no-slip condition is imposed on the channel wall, and along the outflow boundary, zero radial velocity applies. Poiseuille flow is specified at the inlet (see Figure (1)). For the purpose of convergence analysis, consideration is given to a simple geometry that can be effectively meshed into a small number of elements, as it will allow for faster convergence and multiple test runs. This geometry is then subject to testing using FEM code at Δt is $O(10^{-2})$ and the time procedure is checked for convergence to a steady state using relative norms, provided that it meets the appropriate tolerance criteria, which is 10^{-6}

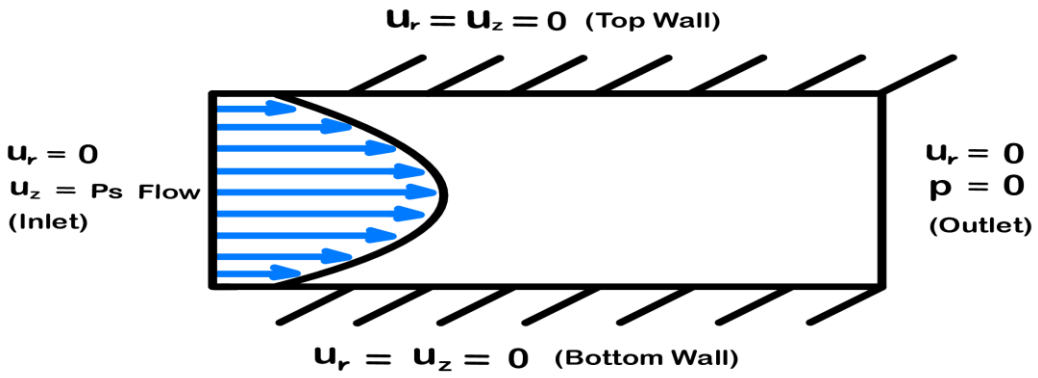

Figure 1: Schema for flow problem, boundary conditions

4. Numerical results and discussion

In the current study, the effects of artificial compressibility on the convergence level based on two different tensors, T_{gv} and T_{rd}, are presented. Here, the influence of β_{ac} on the solution components (velocity and pressure) under T_{gv} is presented in Figure (2) for different settings of $\beta_{ac} = 10,100,1000$ and fixed value $Re = 1$. The results reveal that the rate of convergence is increased as the value of β_{ac} is decreased.

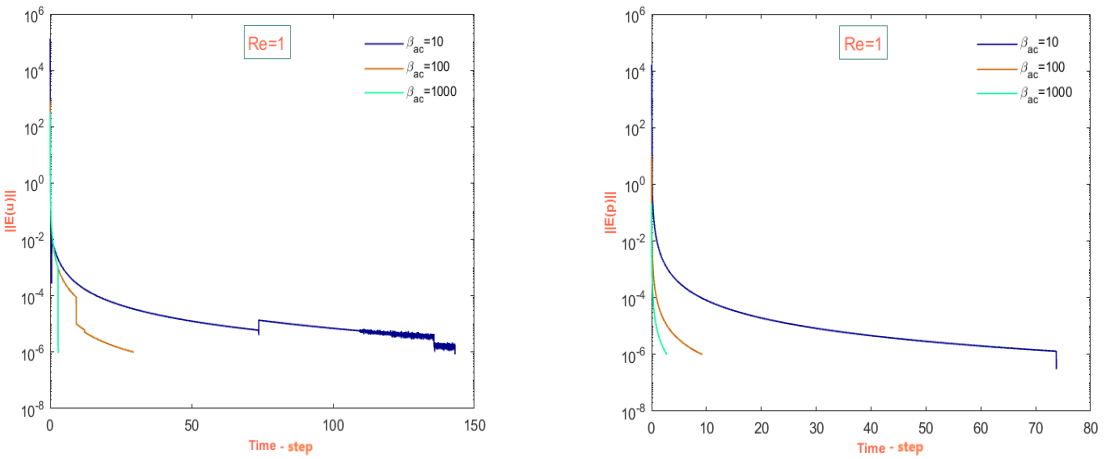

(a) (b)

Figure 2: Convergence of velocity and pressure components, β_ac-various, Re=1.

Figure (3) provides a comparison between velocity and pressure convergence by using T_{gv} and T_{rd}, which depends on the time size by the effect of the β_{ac} parameter. The results show a superior rate of convergence for all solution components within the deformation tensor T_{rd} compared to the T_{gv} tensor at $\beta_{ac} = 100$ and $Re = 1$ (see Figures (3a, 3b)). We noticed that, with a small value of β_{ac}, the convergence of velocity and pressure becomes more difficult and requires a larger number of iterations. Figures 3c and 3d introduce a similar test with $\beta_{ac} = 15$ and $Re = 1$. In this situation, the results diverge with the deformation tensor T_{gv}, while an opposite feature appears under the T_{rd} tensor, indicating the efficiency of using the deformation tensor T_{rd}.

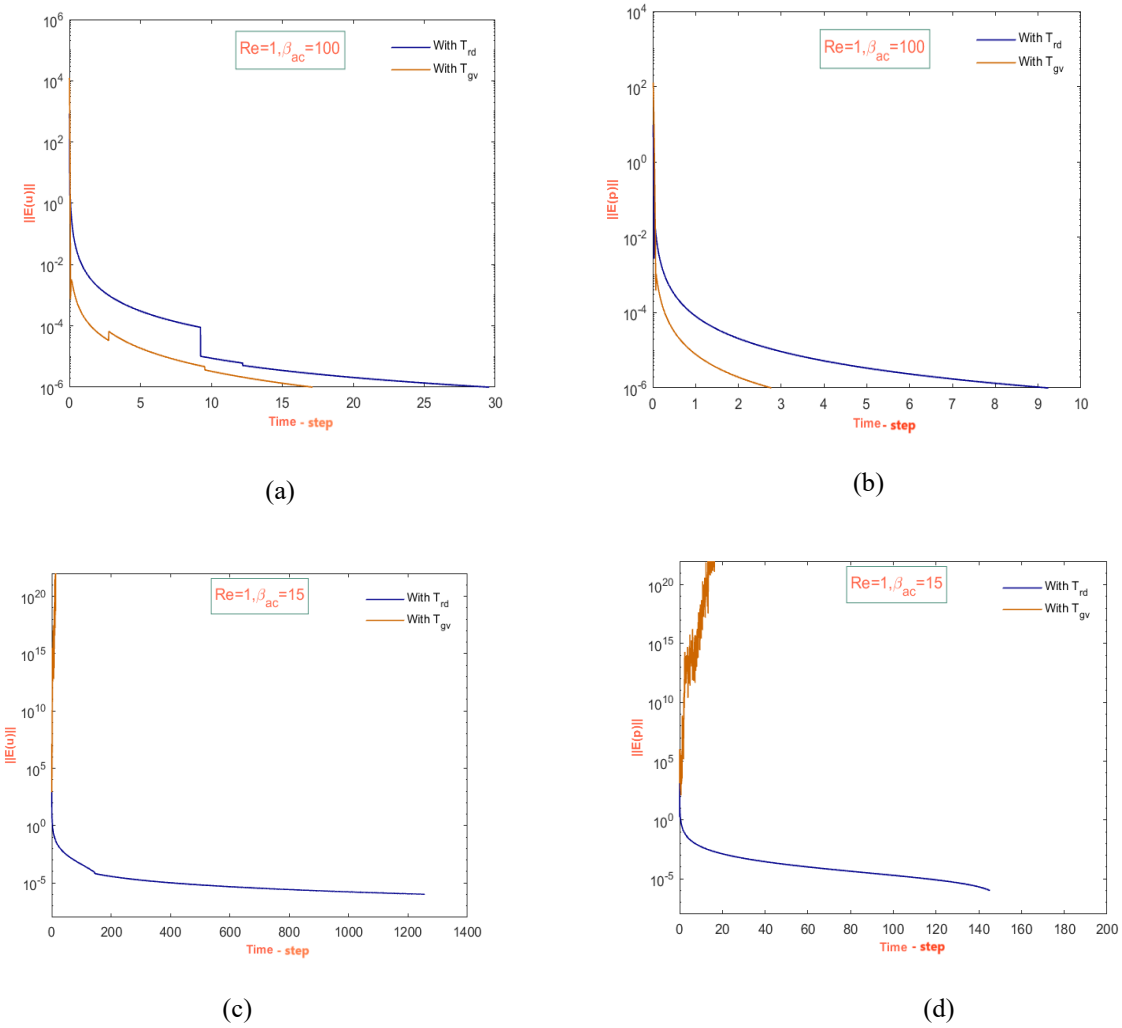

Figure 3: The comparison of velocity and pressure at β_ac-various, Re=1 by using T_rd and T_gv.

Table 1, shows the critical value of β_{ac} by using T_{rd} and T_{gv}, as well as the number of time-step required for convergence. The findings reveal that for both cases, the critical levels of β_{ac} are $\beta_{ac} = 16$ (T_{gv}) and $\beta_{ac} = 0.025$ (T_{rd}). Notably, for the T_{gv} tensor and higher levels of β_{ac}, the level of time-step increments of velocity and pressure decreases than to the T_{rd} instance. From comparing the values from the result, we can note that, by using T_{rd}, we obtain better results compared to those under T_{gv}, which indicates the effect of the spin tensor in T_{gv} on the solution.

Table 1: Critical β_ac and Convergence rate: with T_gv vs T_rd: Re=1.

Along	With T_{gv}	With T_{rd}
Critical β_{ac}	$\beta_{ac} = 16$	$\beta_{ac} = 0.025$
Convergence rate	Pressure=1266.02	Pressure=67964.07
Time- step	Velocity=2338.98	Velocity=23318.85

The rate of convergence for axial velocity and pressure components is provided in Figure (4) for both tensors T_{gv} and T_{rd} based on two different values of the artificial compressibility parameter $\beta_{ac} = 16$ and $\beta_{ac} = 0.025$, respectively, and fixed $Re = 1$. Generally, with T_{gv},

the level of time steps is much lower than that with T_{rd}, so the level of convergence of solution components is faster with the T_{gv} tensor.

Our particular interest in this investigation is to study the critical level of the Reynolds number(Re). Obviously, reaching a high level of Re is a very difficult and interesting issue; thus, we paid attention to determining that level of Re. The anticipated finding is that the level of time steps increases as Re increases. From Figure (5), it can be seen the results of the convergence of pressure and velocity are illustrated at fixed $\beta_{ac} = 100$ and with various levels of Re. Figure 5(a-c) shows that the level of convergence for velocity is higher than pressure; pressure convergence is smoother than velocity convergence. Because of the nonlinear nature of the momentum equation encountered in numerical solutions of velocity behavior, one can observe that the highest value Reynolds we have reached is $Re = 37$ in our investigation.

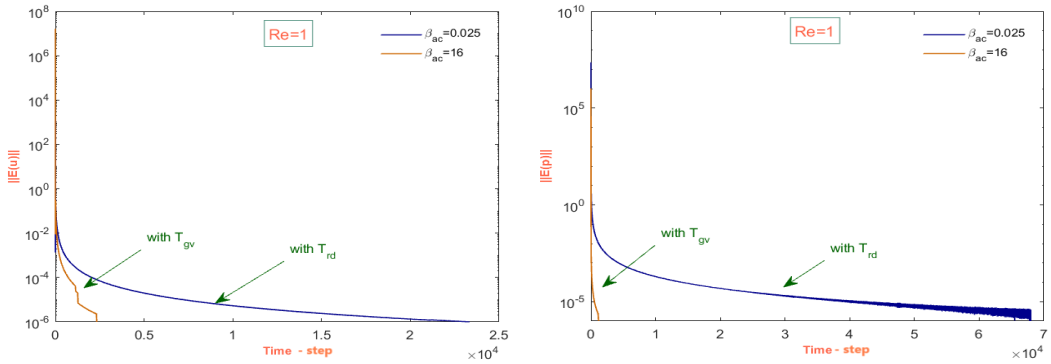

(a) (b)

Figure 4: Critical β_ac and Convergence rate: with T_gv vs T_rd: Re=1.

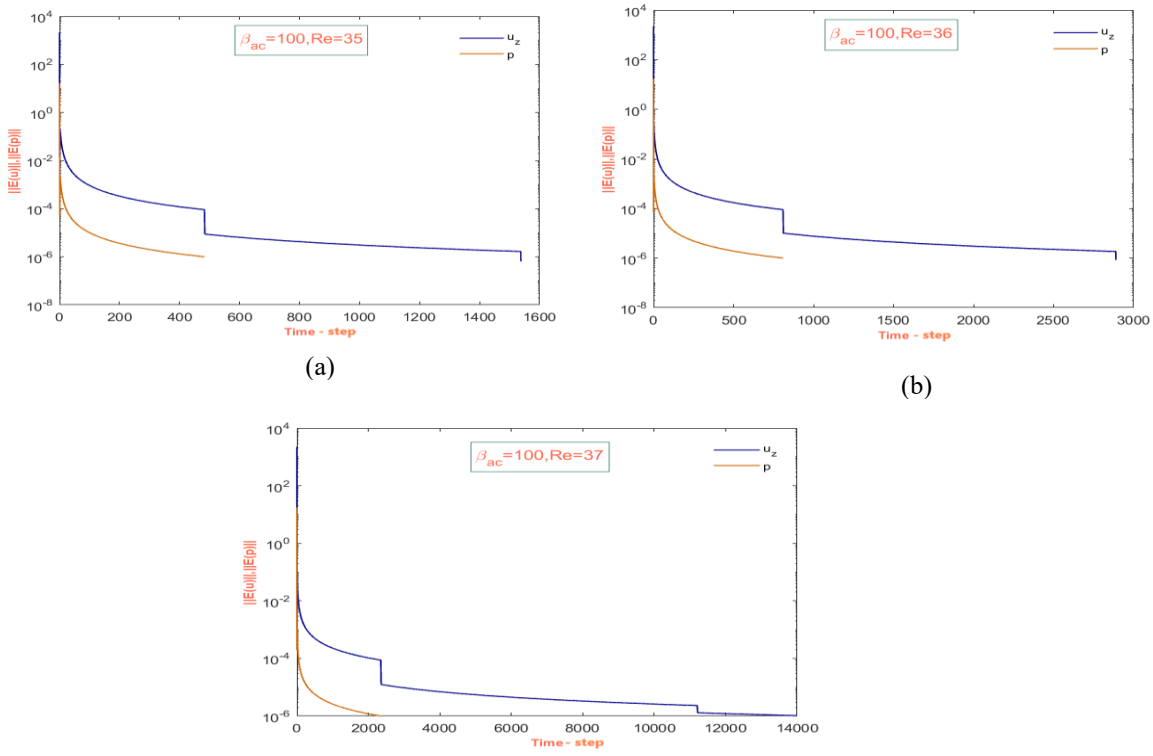

(a)

(b)

(c)

Figure 5: Velocity and Pressure convergence, $\beta_{ac} = 100$, Re variation.

Furthermore, Table 2 provides the critical Reynolds number (Re) for both tensors T_{gv} and T_{rd} at fixed $\beta_{ac} = 100$. From the results, one can see that a high level of Re is observed with T_{rd} compared to T_{gv}, around $Re \sim O(37)$ for T_{rd} and $Re \sim O(7)$ for T_{gv}. More details are provided in Figure(6), where one can see that the convergence of solution components with T_{gv} and critical Re is faster than that with T_{rd}. The rate of deformation significantly influences the level of convergence.

Table 2: Critical Re and Convergence rate: with T_{gv} vs T_{rd}: β_{ac}=100.

Along	With T_{gv}	With T_{rd}
Critical Re	$Re_{crit} = 7$	$Re_{crit} = 37$
Convergence rate (Time -step)	Pressure=1.77	Pressure=2350.38
	Velocity=3457.64	Velocity= 14000

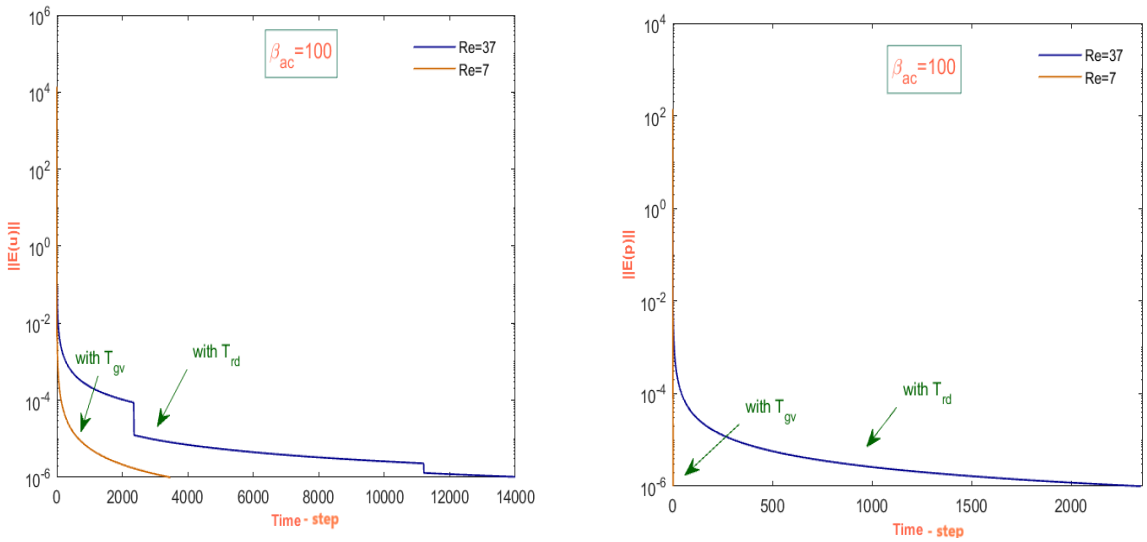

(a) (b)

Figure 6: Critical Re and Convergence rate: with T_gv vs T_rd: β_ac=100.

The comparison between the results of the effect of T_{rd} and T_{gv} on improving the solution will be illustrated in Figure(7).

Figure (7) investigates the level of convergence of velocity and pressure. It also uses two different values of $Re = 1, 7$ and a fixed $\beta_{ac} = 10$, by using both settings of tensors T_{rd} (Figure(7a, 7b)) and T_{gv} (Figure(7c, 7d)). The results reveal that the rate of convergence for both solution components with the T_{rd} tensor is faster than that with the T_{gv} tensor, and a significant difficulty with a high level of Re due to the effect of the antisymmetric part of T_{gv}. In addition, we can note that, for low levels of β_{ac}, an opposite feature occurs (see Figure(4)). In conclusion, we can say that, using the T_{rd} tensor with low β_{ac} is better than utilizing the T_{gv} tensor; in contrast, the T_{gv} tensor is optimal with a high β_{ac}.

Figure (8) illustrates the behavior of velocity components when the Reynolds number is increased using T_{rd} and T_{gv}. The results demonstrate that when using T_{gv} in Figure (8a), the results diverge for values of Re greater than 7, and when using T_{rd} in Figure (8b), the results diverge when Re exceeds 37.

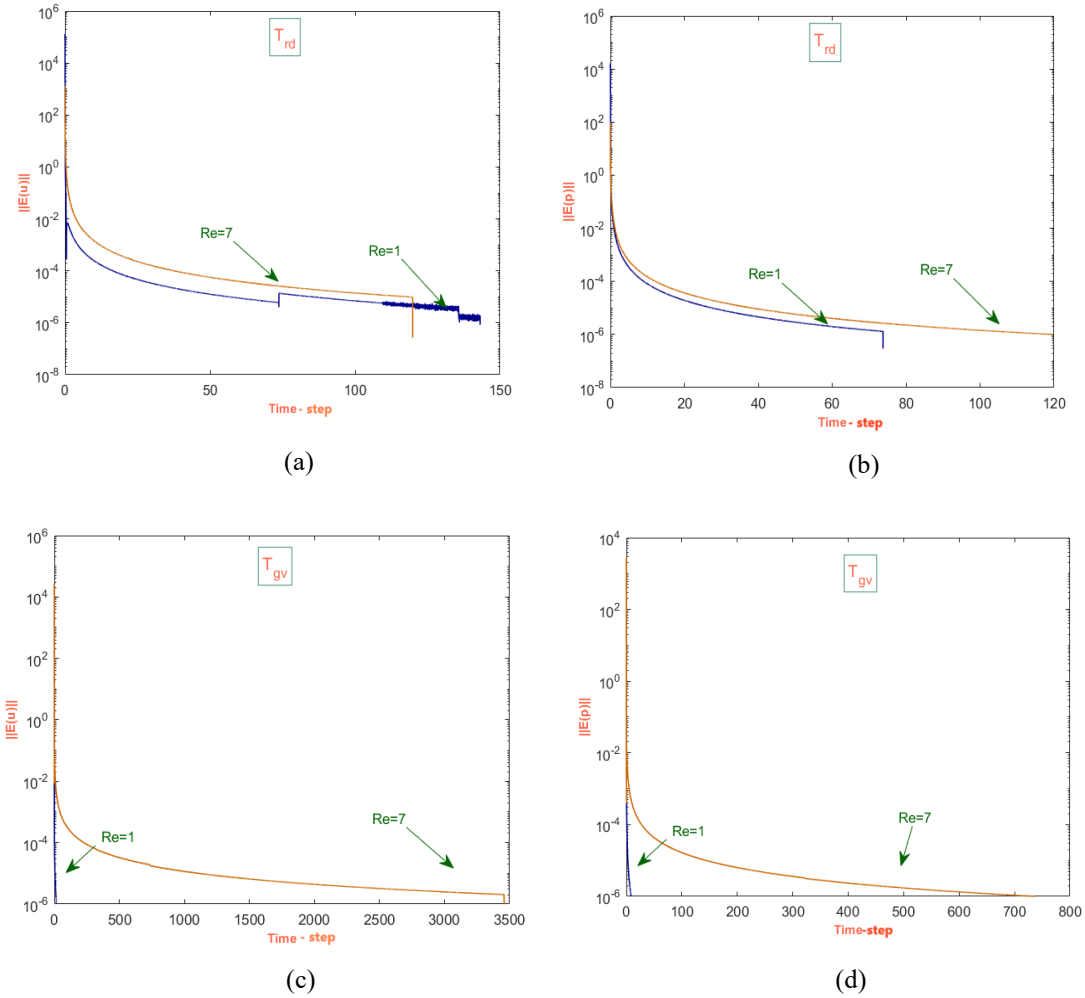

Figure 7: The comparison convergence of velocity and pressure with Re-various and β_ac=10 using the two types T_rd, T_gv.

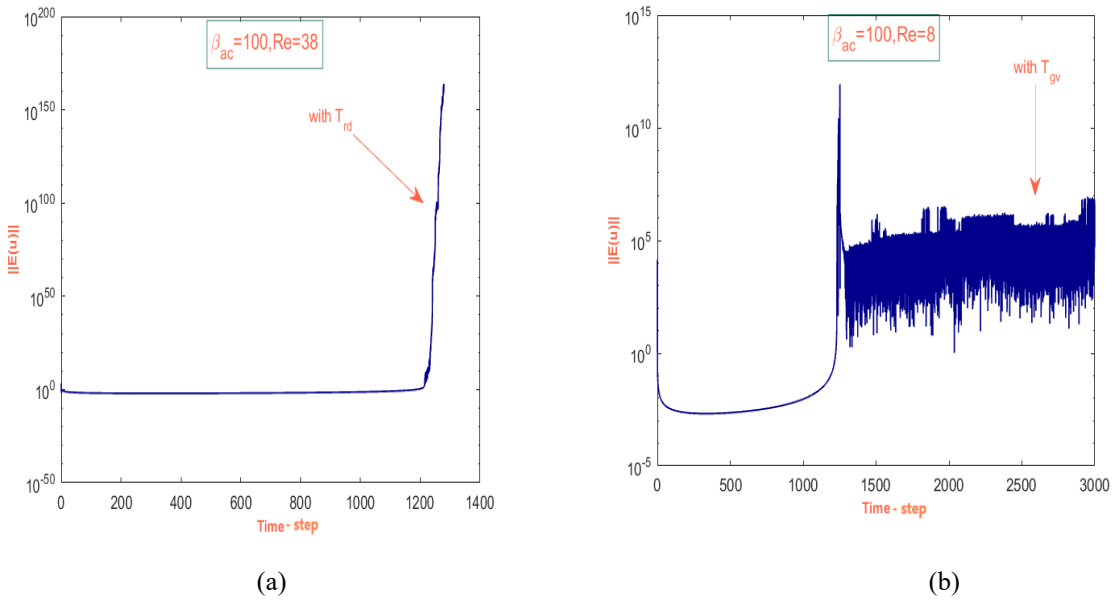

Figure 8 : The comparison of velocity at convergence by using the two types T_rd, T_gv.

5. Conclusions

In this article, the Navier-Stokes equations that govern the fluid flow in a cylindrical coordinate system are solved effectively using the artificial compressibility technique within the finite element method. This study covers the analysis of these equations with two formulations of viscous stress tensor: rate deformation tensor (T_{rd}) and velocity gradient tensor (T_{gv}). The numerical results under both settings of stress tensor are presented to show the effect of various parameters on the rate of convergence of solution components. In this context, we investigated the highest values of the Reynolds number that can be accessed and the effect of Re and β_{ac} within both stress tensors. Improve the solutions and get fast convergence by using the artificial compressibility parameter (β_{ac}) is conducted as well. The main findings of the present study reflect that there is a strong relationship between the artificial compressibility parameter (β_{ac}) and stress tensor. In this matter, we found that a high level of β_{ac} with T_{rd} tensor or a low level of β_{ac} with T_{gv} tensor is enough to make a significant improvement in the level of solution convergence. To confirm the findings, we compared the results obtained in this article with the numerical results obtained in our previous paper, [6]. From this comparison, we can say that we were able to reach the number of Re of higher and reach the smallest level of β_{ac} than the previous study, [6].

References

[1] OC. Zienkiewicz and R. L. Taylor, "The finite element method for solid and structural mechanics," Elsevier, 2005.

[2] G. K. Batchelor, "An introduction to fluid dynamics," Cambridge University Press, 2000.

[3] F. M. White and H. Xue, "Fluid Mechanics," McGraw-Hill New York, 2003.

[4] OC. Zinenkiewicz and R. L. Taylor, "The Finite Element Method," McGraw-Hill, Singapore, vol. 1, 1989.

[5] R. L. Taylor, "The Finite Element Method," vol. 1, 2000.

[6] B. K. Jassim and A. H. Al-Muslimawi, "Numerical analysis of Newtonian flows based on artificial compressibility AC method," *Journal of Al-Qadisiyah for Computer Science and Mathematics,* vol. 9, no.2, pp. 115-128, 2017.

[7] W. F. Carroll, "A primer for finite elements in elastic structures," John Wiley \& Sons, 1998.

[8] G. Nugroho, A. Ali and K. Z. A. Karim, "A class of exact solutions to the three-dimensional incompressible Navier--Stokes equations," *Applied Mathematics Letters,* vol. 23, pp. 1388-1396, 2010.

[9] P. Tait, "HMSO, " London, 1888.

[10] Y. Qin, Y. Wang, Y. Hou and J. Li, "An unconditionally stable artificial compression method for the time-dependent groundwater-surface water flows," *Numerical Methods for Partial Differential Equations,* vol. 39, no. 5, pp. 3705-3724, 2023.

[11] N. Bassou Khouya, N. Mofdi El-Amrani and M. Seaid, "A Conservative and Monotone Characteristic Finite Element Solver for Three-Dimensional Transport and Incompressible Navier-Stokes Equations on Unstructured Grids," *Communications in Computational Physics,* vol. 31, no. 1, pp. 224-256, 2022.

[12] N. E. Kadri and A. Chillali, "A finite element method for compressible and incompressible flows," *SN Applied Sciences,* vol. 2, no. 2, p. 1-14, 2020.

[13] B. R. Hodges, "An Artificial Compressibility Method for 1D Simulation of Open-Channel and Pressurized-Pipe Flow," *Water,* vol. 12, no. 6, pp. 1727, 2020.

[14] S. N. Leloudas, G. N. Lygidakis, N. Georgios, A. I. Delis and I. K. Nikolos, "An artificial compressibility method for axisymmetric swirling flows," *Engineering Computations, v*ol. 38, no. 10, pp. 3732-3767, 2021.

[15] P. R . McHugh and J.D. Ramshaw, "Damped artificial compressibility iteration scheme for

implicit calculations of unsteady incompressible flow," *International Journal for numerical methods in fluids,* vol. 21, pp. 141-153, 1995.

[16] E. Shapiro and D. Drikakis, "Artificial compressibility, characteristics-based schemes for variable density, incompressible, multi-species flows. Part I. Derivation of different formulations and constant density limit," *Journal of Computational Physics, v*ol. 210, no. 2, pp. 584-607, 2005.

[17] Z. Si, G. Xiaonan and Y. Wang, "A modified characteristics projection finite element method for the non-stationary incompressible thermally coupled MHD equations," *Mathematical Methods in the Applied Sciences,* vol. 46, no. 16, pp. 17422-17460, 2023.